Yonsei University – Shizuoka University

Students Workshop 2012

Proceedings

August 24, 2012

Shizuoka University, Hamamatsu, Shizuoka

Program

Yonsei University – Shizuoka University Students Workshop 2012

August 24 (Fri), 2012 at Shizuoka University, Japan

Program

10:00-10:30 **Registration**

10:30-10:40 **Opening Remark**

10:40-11:10 O-01 **(Invited)**

Development of Interactive Nanomanipulators Based on Scanning Probe Microscopes

Professor Futoshi Iwata

11:10-11:25 O-02

High Spatial Resolution Luminescence Microscopy with Direct Electron Beam Excitation for Dynamic Live Cell Imaging ・・・・・・・・11

Yasunori Nawa, W. Inami, A. Chiba, A. Ono, A. Miyakawa, Y. Kawata, S. Lin, and S. Terakawa (Shizuoka University)

11:25-11:40 O-03

Refractive Media Flatness Measurement by Phase Shifting Digital Holography ・・・・・・・・13

Sungbin Jeon, Janghyun Cho, Do-Hyung Kim, No-Cheol Park (Yonsei University)

11:40-11:55 O-04

Deep-UV Surface Plasmon Resonance for the Enhancement of Fluorescence Excitation ・・・・・・・・15

Masakazu Kikawada, A. Ono, W. Inami, and Y. Kawata (Shizuoka University)

11:55-12:10 O-05

Air Gap Control System for High Speed Plasmonic Lithography with Solid Immersion Lens Optical Head ・・・・・・・・17

Guk-Jong Choi, Won-Sup Lee, Taeseob Kim, Geon Lim, No-Cheol Park (Yonsei University)

12:10-13:45 **Lunch**

13:45-14:00 O-06

Micro-Processing of HeLa Cells with Electron Beam ····· 19

Ken Watanabe, W. Inami, Y. Kawata (Shizuoka University)

14:00-14:15 O-07

Development of a MEMS-based Wear Tester ····· 21

Shin-Sung Yoo, Dae-Eun Kim (Yonsei University)

14:15-14:30 O-08

The Numerical Analysis of Intensity Distribution of Light Excited by Electron Beam in a Luminescent Film ····· 23

Masahiro Fukuta, W. Inami, A. Ono, and Y. Kawata (Shizuoka University)

14:30-14:45 O-09

3D Thickness Profile Measurement of a Metal Film Using a Film Removal Process ····· 25

Hang-Eun Joe, Dae Su Kim, Sang Jo Lee, Byung-Kwon Min (Yonsei University)

14:45-15:00 **Coffee Break**

15:00-15:15 O-10

Development of Optically Controllable Electrophoresis with a Photoconductive Substrate ····· 27

Taiki Nagashima, W. Inami, and Y. Kawata (Shizuoka University)

15:15-15:30 O-11

Image Reconstruction for Potable Digital Holographic Microscopy Using Glass Phase Shifter ····· 29

JaeHyeong Park, Janghyun Cho, Sungbin Jeon, Sang Jo Lee, Kyung Soo Lee (Yonsei University)

15:30-15:45 O-12

Measurement of Electron Transmittance of Fluorescent Thin Film with a High Electron Stopping Power Layer ····· 31

Takuya Miyazawa, Y. Nishimura, W. Inami, Y. Kawata (Shizuoka University)

15:45-16:00 **Closing Remark**

Proceedings

High spatial resolution luminescence microscopy with direct electron beam excitation for dynamic live cell imaging

Yasunori Nawa[1], Wataru Inami[2, 3], Atsushi Ono[2, 3], Aki Miyake[3, 4], Sheng Lin[5], Yoshimasa Kawata[1, 3, 4*], and Susumu Terakawa[3, 5]
[1] Graduate School of Science and Technology, Shizuoka University
[2] Division of Global Research Leaders, Shizuoka University,
[3] CREST, Japan Science and Technology Agency, Japan
[4] Department of Mechanical Engineering, Shizuoka University
[5] Medical Photonics Research Center, Hamamatsu University School of Medicine
[*]3-5-1Johoku, Naka, Hmamatsu, Shizuoka 432-8561, Japan
TEL: +81-53-478-1069
e-mail: kawata@eng.shizuoka.ac.jp

Abstract

We have developed a direct electron beam excitation assisted optical microscope with a resolution of a few tens of nanometers. The microscope is a combination of a fluorescence microscope and a scanning electron microscope, and it enables dynamic observation of specimens in liquids with high spatial resolution. This technique is also used for live cell imaging under physiological condition.

1. Introduction

Nano-imaging of specimens in liquids is highly required in the wide range of physical, chemical, and biological applications. Especially imaging biological specimens in cells is crucial for a deeper understanding of cell functions. Fluorescence microscopy has been widely used to analyze the dynamic behavior of cellular elements in living cells, because stained molecules of interest in the specimens can be imaged with high contrast. However, the spatial resolution of the standard fluorescence microscope is limited by the diffraction limit of the light.

Recently several approaches to analyze nanostructures in cells under physiological condition are introduced. These techniques allow to extend the spatial analysis beyond the limit of the optical microscopy.

Here, we propose a direct electron beam excitation assisted optical microscope (D-EXA microscope) for high spatial resolution live cell imaging. The microscope is one of the super-resolution fluorescence microscopes combining a scanning electron microscope (SEM) with a fluorescence microscope. We observed ZnO nanoparticles as a fluorescent material, and demonstrated the application to live cell imaging in culture solution using a prototype D-EXA microscope.

2. Principle of the D-EXA microscope

Figure 1 shows the principle of the D-EXA microscope.

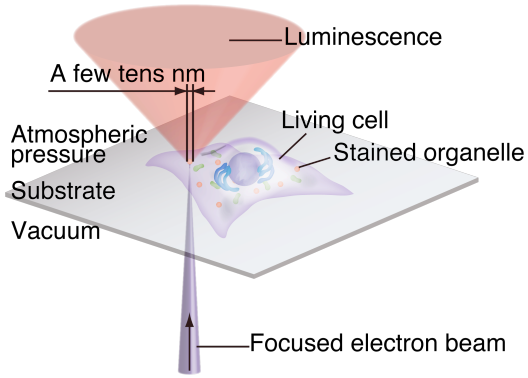

Fig. 1. The principle of the D-EXA microscope. A focused electron beam directly excites cathodolumiescence in the specimens through the thin film. A spatial resolution of a few tens of nanometer is achieved.

Specimens are directly placed on a thin film and stained with fluorescent materials. Fluorescent materials in the specimens are directly excited with a focused electron beam through the thin film.

High spatial resolution is realized, because the focused electron beam can be focused to an area of a few tens of nanometers in specimens.

Since the thin film separates the vacuum

from the environment such as air or liquid, the specimens do not need to be in vacuum and it is possible to observe the dynamic behavior of live cells under various conditions. Cathodoluminescence images are reconstructed with raster scanning of the electron beam.

3. The spatial resolution of the D-EXA microscope

Figures 2A and 2B show luminescence images acquired with the D-EXA microscope and a conventional epi-fluorescence microscope under atmospheric pressure, respectively. The particle size is 100 nm. The ZnO nanoparticles in figure 2A are resolved more clearly compared to figure 2B.

Figures 2C and 2D show line profiles of the region between the arrows in figures 2A and 2B. The D-EXA microscope is able to distinguish each ZnO nanoparticle. The spatial resolution of the D-EXA microscope is greater than 100 nm.

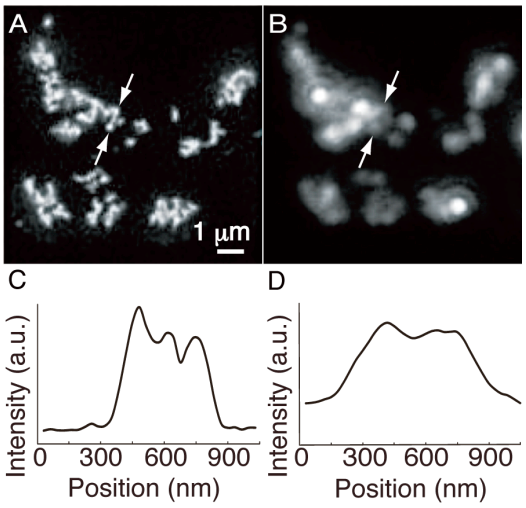

Fig. 2. Luminescence images of 100 nm ZnO nanoparticles. (A) A cathodoluminescence image acquired with the D-EXA microscope. (B) A fluorescence image excited with UV wavelength in epi-fluorescence microscope. (C, D) The luminescence distribution between the arrows in figures 2A and 2B respectively.

4. Dynamic live cell imaging

An electron beam excites auto-fluorescence in biological cells. First, we thus observed auto-fluorescence of the cells without any treatments such as fixing and staining processes.

Figures 3A and 3B show the auto-fluorescence image acquired with the D-EXA microscope and a phase contrast microscope image of living MARCO-expressing CHO cells in culture solution. In figure 3A, the shape of each cell was clearly recognized and some bright spots were observed in cells. We believe that the bright spots indicated with arrows were auto-fluorescence of intracellular granules and light-grey regions were auto-fluorescence of cell membranes. It is clearly demonstrated that the D-EXA microscope is useful tool for observation of living biological cells in physiological conditions.

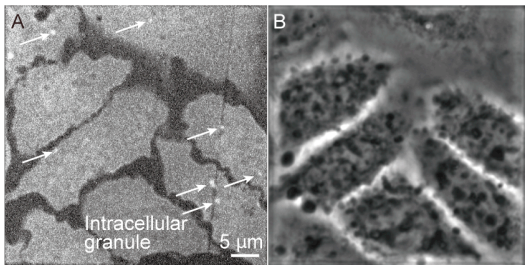

Fig. 3. Observation results of living MARCO-expressing CHO cells in culture solution. (A) An auto-fluorescence image acquired with the D-EXA microscope. (B) A phase contrast microscope image of the cells.

5. Conclusion

We have developed the D-EXA microscope as one of the super-resolution fluorescence microscope with direct electron beam excitation. A spatial resolution greater than 100 nm was achieved. Living cells were successfully observed in water based solution with high spatial resolution. The D-EXA microscope can be applied for the analysis of cell functions staining with fluorescent materials such as ZnO.

Reference

[1] Y. Nawa, W. Inami, A. Chiba, A. Ono, A. Miyakawa, Y. Kawata, S. Lin, and S. Terakawa, Opt. Exp. 20, 5629 (2012).

Refractive media flatness measurement by phase-shifting digital holography

Sungbin Jeon, Janghyun Cho, Do-Hyung Kim, No-Cheol Park*

Department of Mechanical Engineering Center for Information Storage Device
50 Yonsei-ro, Seodaemun-gu, Seoul Korea 120-749
TEL&FAX: +82-2-365-8460
*e-mail: pnch@yonsei.ac.kr

Abstract

Digital holography can be used in various application including the measurement of flatness of surface. In this paper, the transmittive phase-shifting digital holography is used to acquire the surface profile of refractive media with high-resolution.

1. Introduction

One of the applications of digital holography is measuring the surface profile. This interferometric approach has advantages for nano-scale precision, noncontacting and whole-field measurement. In recent years, many methods like Fizeau [1]] and Twyman-Green [2] interferometers were developed. But most of these research were to use the information in reflected object beam. Reflective interferometer can measure any types of media, but it also has the weakness of error of object stage, like angular tilt or roughness of stage. In addition, reflective method can only measure the flatness of surface in one side. To overcome these problem, we propose the transmissive phse-shifting digital holography.

2. Phase-shifting Digital Holography

Phase-shifting digital holography is the method which can eliminate the zero and minus-first order diffracted wave. It requires at least two holograms with phase-different reference wave. From these holograms, the complex amplitude can be easily acquired by calculation [3] The phase distribution obtained from it can be converted into the surface profile or flatness of both side of plate. In addition, phase-shifting digital holography can apply in-line setup, and usable CCD area is much bigger than other off-axis holography method. Thus it can measure large surface at once.

3. Phase-shifting Holographic Flatness Measurement

Figure 1 illustrates the schematic of a system configuration of flatness measurement for refractive media using phase-shifting digital holography. The light

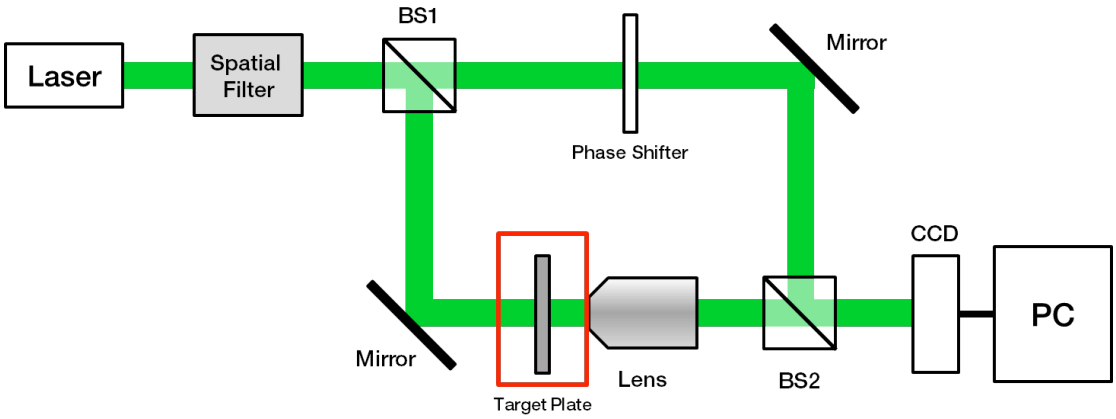

Fig. 1 System configuration of flatness measurement for refractive media using phase-shifting digital holography

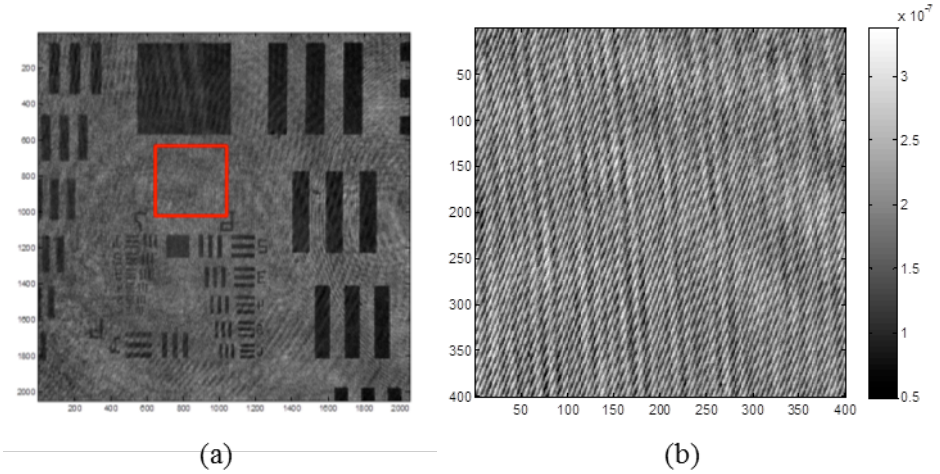

Fig. 2 (a) Acquired complex amplitude from phase-shifting holography (b) Calculated surface profile of the area denoted in Fig. 2 (a)

source is Nd: Yag laser with a wavelength $\lambda = 532$ nm. The CCD has an array of 2448×2050 pixels, wich is cropped into 2050×2050 due to simplicity in calculation. The size of each pixel is 3.45 μm. The transparent plate is located in object plane to acquire the phase-shifted interference image. To shift the phase of the reference wave precisely, phase SLM is used. The microscopy lens was used to increase the lateral resolution of measurement.

Figure 2 shows the experiment result using the proposed setup. The BK7 glass plate printed with USAF chart was used. In this paper, 2-step phase-shifting holography with phase difference of $\pi/2$. The complex amplitude acquired from holograms is shown in Fig. 2(a). Figure 2(b) is the surface profile of the glass plate of partial area. Since the glass is not well-polished, the thickness difference of surface is up to 350nm.

4. Conclusion

In this research, the flatness of refractive media plate is measured using transmissive phase-shifting digital holography. Using this setup the surface profile can be obtained fast, and less error compared with conventional interferometric method.

Reference

[1] D. Bhattacharyya, A. Ray, B. K. Dutta, and P. N. Ghosh, "Direct measurement on transparent plates by using Fizeau interferometry," Optics & Laser Technology **34**, 93-96 (2002).

[2] O. Kwon, J. C. Wyant, and C. R. Hayslett, "Rough surface interferometry at 10.6 μm," Appl. Opt. **19**, 1862-1869 (1980)

[3] I. Yamaguchi and T. Zhang, "Phase-shifting digital holography," Optics letters **22**, 1268-1270 (1997)

Deep-UV Surface Plasmon Resonance for the Enhancement of Fluorescence Excitation

Masakazu Kikawada[1], Atsushi Ono[2,3], Wataru Inami[2,3], and Yoshimasa Kawata[1,3*]

[1]Faculty of Engineering, Shizuoka Univ.
[2]Division of Global Research Leaders, Shizuoka Univ.
[3]CREST, Japan Science and Technology Agency, Japan
3-5-1, Johoku, Naka, Hamamatsu 432-8561, Japan
TEL&FAX: +81-53-478-1076
[*]e-mail: Kawata@eng.shizuoka.ac.jp

Abstract

We present the enhancement of fluorescence excitation with deep ultra-violet surface plasmon resonance (DUV-SPR). It is found that aluminum is good material to excite SPR with DUV light. We also demonstrate fluorescence enhancement of quantum dots with field enhancement effect of DUV-SPR.

1. Introduction

Recently, surface plasmon resonance (SPR) has attracted much attentions in various fields such as optical bio-sensors, high efficient LED, solar panels, etc., because it enables to enhance the electric field of incident light by several tens times. Many applications of SPR using visible light or near infrared light have been reported [1]. The techniques of SPR in red or infrared region have been well established.

SPR in DUV region are also reported some groups [2]. These researches achieved nanoscale resolution beyond the diffraction limit of light. We also reported the enhancement of photoelectron emission [3]. The photoelectric current was enhanced 9 times due to field enhancement by DUV-SPR.

2. Metal for DUV-SPR Excitation

The permittivity of metal is very important to excite DUV-SPR. It is necessary that its real part should be negative and its imaginary part to should be small imaginary part. We use aluminum to excite DUV-SPR. Figure 1 (a) and (b) show permittivity dispersion of real part and imaginary part respectively. Aluminum is a good material to excite SPR in DUV region. The metals such as gold and silver, which are good materials to excite SPR in visible region, can't be used in DUV, because they have large absorption in the wavelength region.

3. Experimental set-up for DUV-SPR excitation and fluorescence enhancement

We evaporated aluminum of 26 nm thickness on a prism surface at the condition of Kretchmann configuration shown in figure 2. A fluorescent material is coated on the aluminum thin film.

DUV laser is irradiated boundary between prism and the aluminum thin film. We measured the intensity of reflected light and fluorescence with changing incident angle.

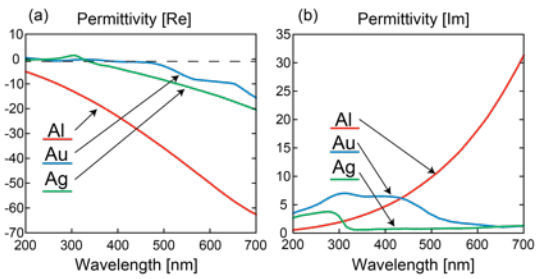

Fig. 1. (a) Permittivity of real part and (b) Permittivity of imaginary part. Red line is aluminum. Blue line is gold. Green line is silver.

4. Results of reflectance and fluorescence intensity

Figure 3(a) shows experimental result of reflectance dependence on the incident angle. Red line and blue line indicate *p*-polarization and *s*-polarization, respectively. Reflectance drastically decreases around 49 degrees at *p*-polarization. On the other hand, reflectance is almost constant at *s*-polarization. In this result, we successfully excited SPR in DUV region.

Figure 3(b) shows calculation result of reflectance. Blue line indicates reflectance at the aluminum thickness of 26 nm. Reflectance drastically decreases around 44 degrees. The angle which reflectance decreases of experimental result and the one of calculation result don't correspond in this result. Moreover, reflectance of experimental result and calculation result don't correspond.

We calculated reflectance considering with the condition that the aluminum surface was oxidized, because, aluminum is easily to oxidized at the atmosphere. Red line of figure 3(b) indicates reflectance of 19 nm aluminum thickness and 5 nm oxidized of aluminum. Experimental result shows good agreement with calculation result.

We demonstrated DUV-SPR excitation for fluorescent enhancement. We used quantum dots as a fluorescent material. This material absorbs the light, the wavelength of which is shorter than 370 nm and emission wavelength is 380 nm. quantum dots was spin-coated on aluminum thin film.

Figure 4(a) shows fluorescence intensity dependence on the incident angle. Fluorescence intensity maximized at the 49 degrees with *p*-polarization excitation. On the other hands, fluorescence was constant with *s*-polarization excitation.

In these results, fluorescence intensity is enhanced by the excitation of DUV-SPR. The maximum intensity of fluorescence in *p*-polarization is enhanced to 24 times compared with that in *s*-polarization. We measured the fluorescent spectrum shown in figure 4(b). The emission spectrum has the peak at 380 nm wavelength with *p*-polarization. This peak wavelength is corresponding to the emission wavelength of quantum dots. We may concluded that we succeeded fluorescence enhancement of

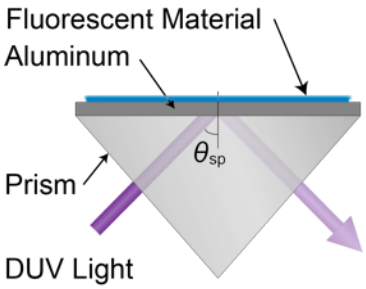

Fig. 2. Kretchmann configuration

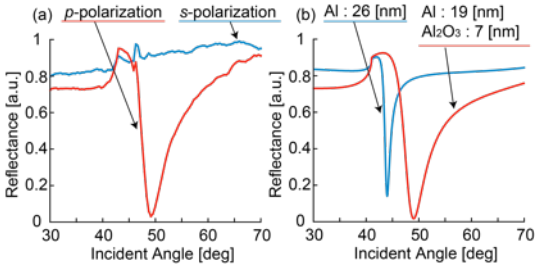

Fig. 3. Reflectance (a) experimental result and (b) calculation result

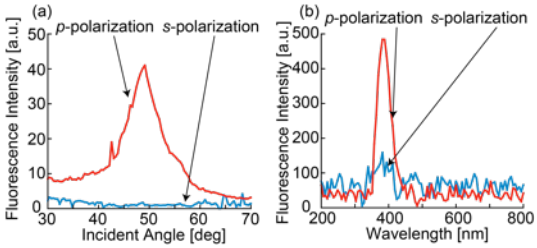

Fig. 4. (a) Fluorescence intensity (b) Spectrum quantum dots using DUV-SPR.

5. Conclusion

We successfully excited DUV-SPR and achieved 24 times enhancement of fluorescence intensity of Q-dot by DUV-SPR. The wavelength range of SPR excitation can be extended to the DUV region by using aluminum. DUV has advantage of autofluorescence observation because most cells and organisms emit autofluorescence by DUV illumination.

Reference

[1] K. Tawa, *et. al. OPTICS EXPRESS*, **16**, 9781 (2008).
[2] A. Taguchi, *et. al. Journal of RAMAN SPECTROSCOPY*, **40**, 1324 (2009).
[3] Y. Watanabe, *et. al. JOURNAL OF APPLIED PHYSICS*, **109**, 023112 (2011).

Air gap control system for high speed plasmonic lithography with solid immersion lens optical head

Guk-Jong Choi, Taeseob Kim, Won-Sub Lee, Geon Lim and No-Cheol Park*

Department of Mechanical Engineering Center for Information Storage Device
50 Yonsei-ro, Seodaemun-gu, Seoul Korea 120-749
TEL&FAX: +82-2-365-8460
*e-mail: pnch@yonsei.ac.kr

Abstract

This paper introduces air gap control system of optical head with solid immersion lens (SIL) for high speed plasmonic lithography. In order to achieve nano pattern size, air gap should be remained under 20 nm precisely. In this system, evanescent coupling effect is used for air gap in near field (NF) and the result is about 70 nm pattern size at 100 mm/s.

1. Introduction

Plasmonic lithography is the next generation lithography technology which overcomes a limitation of wavelength and reduces the cost of manufacture. This lithography method uses the nano metallic wave guide causing the surface plasmon resonance (SPR) effect. It can make very narrow lithography patterning in units of tens of nanometer only when distance between the wave guide and photoresist (PR) is within a quarter wavelength of laser source [1]. There have been several attempts to maintain the distance such as an air bearing system in hard disk drive, a contact system with probe and an active air gap control system in near field recording [2-4]. Among these types of system, the active control type has advantages which are less limitation for pattering than the air bearing one and faster patterning speed than the probe one. In this paper, we introduce air gap control for plasmonic lithography and demonstrate the performance of lithography patterning at a speed of 100 mm/s.

2. Air gap control system

We control the air gap between an optical head and a PR. Figure 1 shows the optical head composed of a voice coil motor (VCM) actuator and SIL with the nano metallic wave guide and we use two-wavelength optics with laser sources of 408 nm and 633 nm. It is designed for 408 nm to record pattern. The 633 nm laser is used for detecting the air gap signal.

Figure 2 (a) shows the algorithm of the air gap control system. It has the two key functions. One is an air gap curve. The other is mode switching. The air gap curve is related with the evanescent coupling effect which is depending on degree of the transmission of 633 nm laser in total reflection condition at the bottom of the optical head. The role of the air gap curve is that the optical intensity changes to the air gap. The mode switching is the algorithm which has three modes. First mode is approach mode which is possible for optical head to be closer from far field to NF. Second mode is hand over mode that makes approach of optical head to NF smoothly. These two modes are essential because feedback control is only feasible in NF. Third mode is the air gap control which works by closed loop to maintain the certain

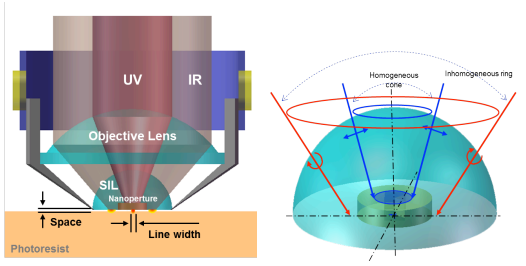

Fig. 1 Optical head with VCM actuator and SIL. Total optical head configuration is left figure and SIL with the nano wave guide is right figure. UV laser source is 408 nm and IR laser source is 633 nm wavelength.

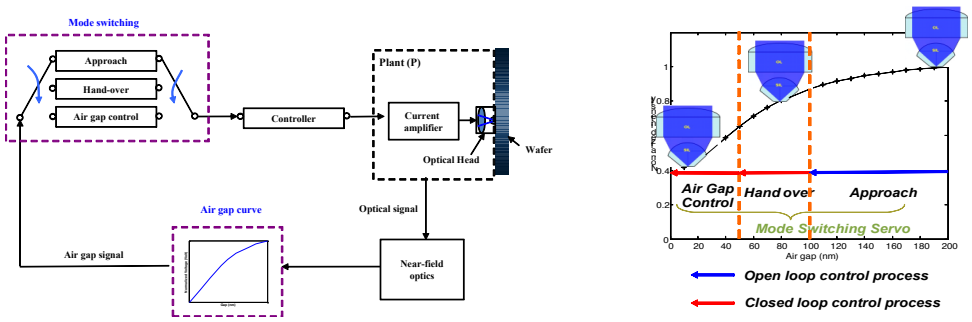

(a) (b)

Fig. 2 Air gap control algorithm. (a) Block diagram of the algorithm and (b) the configuration of the relationship between the mode switching and the gap curve.

air gap. Figure 2 (b) shows the state of the each mode with the air gap curve.

3. Results and Discussion

Figure 3 (a) and (b) show a controlled air gap signal at 20 nm and the performance of lithography patterning, respectively. The line width of the patterning is nearly consistent with the calculated the beam spot of the wave guide which is operated by finite time difference method [4]. The conditions of the experiment are 20 nm air gap and 100 mm/s speed of pattern.

4. Conclusion

In this study, we demonstrate the air gap control system for high speed plasmonic lithography. We control the air gap maintaining 20 nm, and therefore achieve a resolution of ~70 nm with patterning speed of 100 mm/s.

Reference

[1] J.I Lee, M. Van der Aa, C. Verschuren, F. Zijp and M. Van der mark, JJAP. 44 (2005) 3423

[2] W. Srituravanich, L. Pan, Y. Wang, C. Sun, D. B. Bogy and X. Zhang, Nature nanotechnology, 3 (2008) 733

[3] Y. Kim, S. Kim, H. Jung, E. Lee and J. W. Hahn, Optics Express, 17 (2009) 19476

[4] K.S. Park, T. Kim, W.S. Lee, H.E. Joe, B.K. Min, Y.P. Park, H. Yang, S.M. Kang and N.C. Park, JJAP 51 (2012) (accepted)

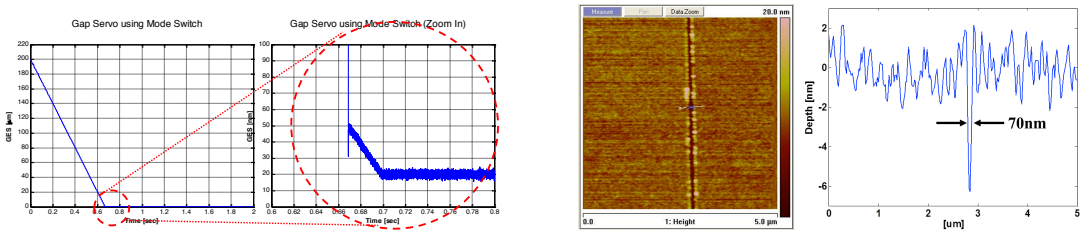

(a) (b)

Fig. 3 Result of the experiment of the plasmonic lithography system. (a) Air gap control at 20 nm and (b) lithography patterning with linewidth 70 nm at 100 mm/s and the same air gap.

Micro-processing of HeLa cells with an electron beam

Ken Watanabe[1], Wataru Inami[2,3], and Yoshimasa Kawata[1,3]

[1]Faculty of Mechanical Engineering, Shizuoka University,
[2]Division of Global Research Leaders, Shizuoka University, [3]JST-CREST
TEL&FAX: +81-53-478-1076
[*]e-mail: kawata@eng.shizuoka.ac.jp

Abstract

Recently, development of micro fabrication for cells and other living tissues are required for biological science. We present characteristic evaluation of cell processing using an electron beam, in order to realize fine fabrication in nanometric region. We succeeded in processing HeLa cells. And in this experiment, we investigated dependence of processing depth and width on accelerating voltage.

1. Introduction

The technologies of cell-processing are studied widely for medicine and biology application. In previous studies, cells are cut by laser-ablation [1]. Figure 1 shows comparison of the resolution of laser and electron beam. Laser processing has the resolution of hundreds of nm-order because the resolution is restricted by the diffraction limit of light. On the ather hand, electron beam has the resolution of tens of nm-order.

We present cell processing using an electron beam. The electron beam can be used for fabricate cells with a nanometric resolution since the electron beam can be focused to a few tens of nanometer. If we can achive processing of tens nano-order, we can get a precision to process ion channel in a cell membrane. This undeveloped technology may accomplish an analysis of medicine for cancer.

In our experiments, we irradiated an electron beam to fixed and dried cells, and investigated dependence of the processing depth and width on accelerating voltage of an electron beam.

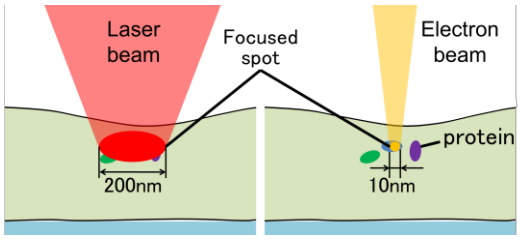

Fig. 1. Resolution of Laser and Electron beam

2. The experimental device for electron beam processing

For irradiating cells with an electron beam, we used scanning electron microscope (SEM). We used HeLa cells which was cultured on a slide glass, and carried out fixation/dry processing in order to process in a vacuum. Figure 2(a) shows the schematic diagram of the cellprocessing experiment. The focused electron beam was scanned in a circle. Figure 2(b) is SEM image of a processed HeLa cell. It was found that the HeLa cell was successfully processed by the focused electron beam.

We changed accelerating voltage of electron beam from 2 kV to 20kV. And the volume of electron forming electron beam were same in all irradiation conditions. When the spot sizes of electron beam were 35 nm and 110 nm, electron numbers were 4.38×10^{8} and 4.44×10^{7} electrons per 1 nm^2.

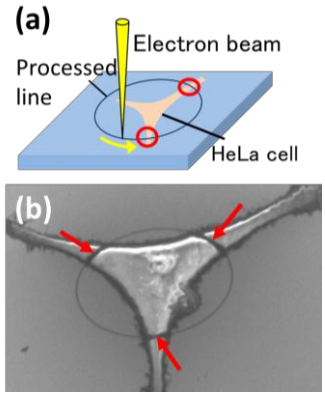

Fig. 2 Electron beam processing for a cell

3. Results and Discussion

After irradiating an electron beam to a cell, we observed the cell with an optical phase microscope and an atomic force microscope (AFM). Figure 3 shows an observation result of a cell before and after irradiation of electron beam of 20 kV accelerating voltage. The cell was processed with the electron beam. In figure, the processed mark was clearly observed. Figure 4 shows a cross-sectional view of the processed cell. The cell become depressed at irradiated area and the processing depth is 135 nm.

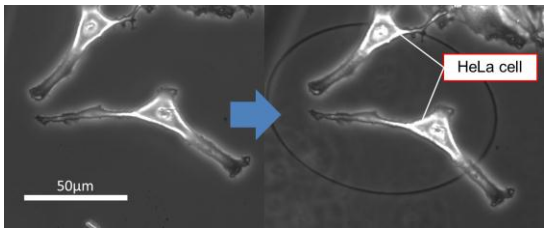

Fig. 3. The phase- contrast microscope images of a cell before and after irradiation of electron beam of 20 kV accelerating voltage

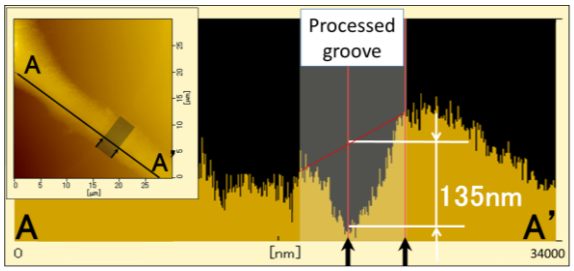

Fig. 4. The results of observation in an atomic force microscopy

The surface deformation of the cell with the electron beam with spot size of 35 nm was observed in the accelerating voltage range from 2 kV to 15 kV. The depth increased with increasing the accelerating voltage. For the electron beam with spot size of 110 nm, the surface of the cell did not deformed with the accelerating voltage of less than 10 kV, and the processing depth increased with the accelerating voltage of more than 10 kV.

Figure 6 shows the processing width dependence on accelerating voltage of an electron beam. The width of the groove processed with the electron beam with increased as the accelerating voltage increased. The depth of the groove processed with an electron beam with spot size of 35 nm is deeper than that with spot size of 110 nm because the energy of the electron beam with spot size of 35 nm is focus to smaller region. The depth became lager as the accelerating voltage increased, peaking around 10 kV.

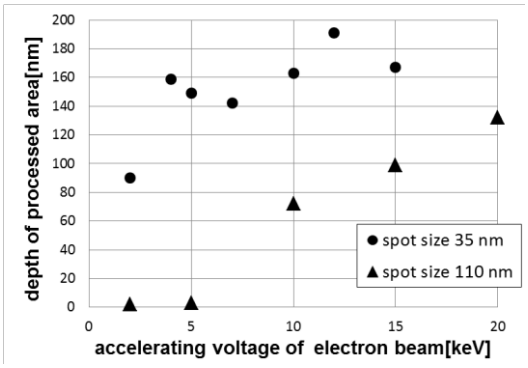

Fig. 5. The depth dependency of irradiation area

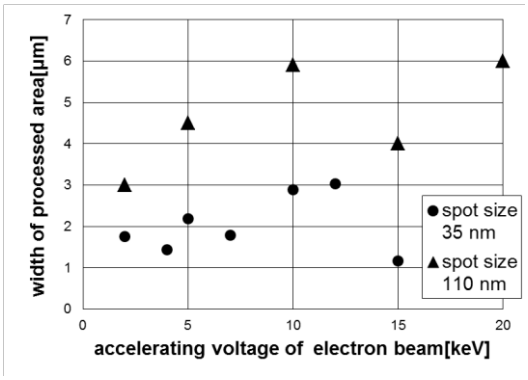

Fig. 6. The width dependency of irradiation area

4. Conclusion

We processed HeLa cells with a focused electron beam. The processing depth increased with higher accelerating voltage and smaller spot. And the processing width increased with higher accelerating voltage and larger spot. A focused electron beam realizes nano processing of cells. We optimize the spot size of electron beam and accelerating voltage to realize finer processing.

Reference

[1]M. W. Berns, J. Aist, J. Edwards, K. Strahs, J. Girton, P. McNeill, J. B. Rattner, M. Kitzes, M. Kitzes, M. Hamme-Wilson, Science, vol.213, pp.505, 1981.

Development of a MEMS-based Wear Tester

Shin-Sung Yoo and Dae-Eun Kim*

School of Mechanical Engineering, Yonsei University,
50 Yonsei-ro, Seodaemun-gu, Seoul, 120-749, South Korea
TEL: +82-2-2123-2822, FAX: +82-2-365-0491
* e-mail: kimde@yonsei.ac.kr

Abstract

Micro-Electro-Mechanical Systems (MEMS) are comprised of silicon-based micro-scale components. In many MEMS applications, it is desirable to have moving parts such as gears, shafts, and bearings. However, due to tribological issues of mechanical components at the micro-scale, the reliability problems must be overcome in order to develop MEMS with moving parts. In this presentation, the design approach for developing a MEMS-based micro-wear tester will be discussed. Particularly, the dynamics of the actuator supporting structure was analyzed using Finite Element Method (FEM). Such a tester is needed to investigate the tribological phenomena at the micro-scale.

1. Introduction

It is well known that when the size of a mechanical component decreases, the effects of surface forces become more important than at larger scales. This is because the ratio of surface area to volume becomes large as the dimensions decrease [1]. Due to these reasons commercialized MEMS devices mostly operate without large sliding motions [2]. Basically, the MEMS components deform or move only slightly so that sliding can be avoided [3]. However, this limits the application of MEMS technology in various fields [4]. In order to overcome this problem, a clear understanding of the friction and wear characteristics at the micro-scale must be established. The motivation of this work was to develop a tester that can be used to investigate the wear behavior of silicon-based micro-components.

Developing a wear tester at the micro-scale is not straightforward. Basic MEMS fabrication processes much be utilized to make the wear tester since the size of the components is quite small. In this work, a new micro-wear tester was designed to improve the demerits of previously developed MEMS tribotester [5].

2. General Design

In a wear test, two components slide against each other under an applied normal load for a given period of time until the surface gets damaged by wear. Thus, it is necessary to design a structure that can support the applied load as well as an actuator that can create the sliding motion. In a MEMS-based micro-wear tester these features must be integrated in a small volume.

Fig. 1 shows the schematic of the newly developed micro-wear tester. The normal load is applied by the top cover which is pressed against the bottom structure. The two components come into contact as the load is applied. The bottom component is designed to deflect when the normal load is applied. Then, the bottom specimen moves in a reciprocating motion by the MEMS actuators that are linked to the bottom component. This motion causes friction to occur at the sliding interface and when this continues for an extended time, the components experience wear.

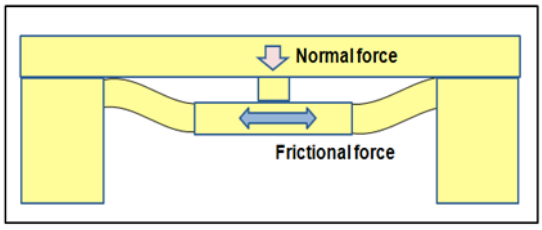

Fig.1 Schematic of the micro-wear tester

3. Structural Analysis

An important consideration in the development of the micro-wear tester shown in Fig. 1 is the integrity of the structure. Since the parts are very small and the linkages are thin, care must be taken to assure that these parts do not break during the wear test. Also, since the components are moving in a reciprocating motion, the dynamics of the system should be controlled so that desirable sliding distance can be attained. For this purpose, FEM analyses were performed to optimize the structural design.

The main design parameters were length and thickness of the linkages. It was found that by properly designing the dimensions of the structure, adequate horizontal displacement could be achieved. Furthermore, stress analysis of the components revealed that the structure was capable of withstanding the forces generated during the wear test.

4. Conclusion

In this research, a micro-wear tester was designed to investigate the tribological characteristics of micro-components. The design of the tester was optimized to produce stable actuation in the desired range of frequency. Also, the dimensions of the structural parts were selected to attain adequate durability of the tester. It is expected that the results of this work will be used to better understand the tribological phenomena at the micro-scale.

5. Acknowledgement

This work was supported by the National Foundation of Korea (NRF) grant by the Korea government (MEST). (No. 2012-0001232)

References

[1] J. G. Guo and Y. P. Zhao, Influence of van der Waals and Casimir Forces on Electrostatic Torsional Actuators, J. Microelectromech. S., 13 (2004) 1027-1035.

[2] http://www.iSuppli.com, MEMS Market Tracker, 2011.

[3] J. A. Williams and H. R. Lee, Tribology and MEMS, J. Phys. D : Appl. Phys., 39 (2006) 201-214.

[4] W. Merlijin van Spengen, MEMS reliability from a failure mechanisms perspective, MIcroelectron. Reliab., 43 (2003) 1049-1060.

[5] Z. Guo, Y. Meng, H. Wu, C. Su and S. Wen, Measurement of static and dynamic friction coefficients of sidewall of bulk-microfabricated MEMS devices with an on-chip micro-tribotester, Sensor Actuator A, 135 (2007) 863-869.

The numerical analysis of intensity distribution of light excited by electron beam in a luminescent film

Masahiro Fukuta[1, 2], Wataru Inami[2, 3], Atsushi Ono[2, 3], Yoshimasa Kawata[1, 3]

[1]Faculty of Engineering Shizuoka University, Japan
[2]Division of Global Research Leaders, Shizuoka University, Japan
[3]CREST Japan Science and Technology Agency, Japan
E-mail: kawata@eng.shizuoka.ac.jp

Abstract

We analyze the spread of cathodoluminescence occurred in the luminescent film. We used the new analysis method that is combined the Monte Carlo simulation and FDTD method. The Monte Carlo simulation analyzes the electron beam scattering and the FDTD method analyzes the light scattering. In addition, we use the energy loss of electrons. As a result, the spot size of cathodoluminescence becomes lower with increasing acceleration voltage.

1. Introduction

The purpose of this research is analyze the spread of cathodoluminescence occurred in the luminescent film by electron beam excitation. To achieve this, we analyze the electron beam scattering through the luminescent film and the light scattering of cathodoluminescence. The electron beam scattering is analyzed by Monte Carlo simulation and the FDTD simulation is analyzed by FDTD method (Finite Difference Time Domain method). We add the energy loss distribution of electrons in order to accurately simulate. This study suggests the new analysis method that combines the Monte Carlo simulation, FDTD method and energy loss distribution of electrons.

2. The analysis method of electron beam scattering and light scattering

We analyze the electron beam scattering by the Monte Carlo simulation [1]. The incident electron goes straight and change angle by colliding with atoms in the luminescent film. The distance between scattering points and the angle calculate by random numbers. The cathodoluminescence is occurred by the energy loses of electrons at scattering process. The creation energy of one electron hole pairs is three times of band gap [2]. Thus, we evaluate the photons excited by electron energy loss by divide energy loss by three times of band gap. We consider the cathodoluminescence as a gathering of point light sources, and we use the dipole emission as the point light source. FDTD method analyzes light scattering of dipoles. We analyze the light scattering for each dipole and we get the light scattering of cathodoluminescence from sum the result of light scattering of each dipole.

3. The placement of light source

In this study, we set the dipoles to the multiple points between the scattering points. We apply the energy loss distribution of electrons to set the dipole

to the multiple points. The energy loss distribution of electrons is shown in figure 1. Figure 2 shows the relationship between photon number and Z-axis position. The photon distribution can approximate the theoretical distribution by set dipoles to multiple points between the scattering points.

4. Analysis result of cathodoluinescence

Figure 3 is the relationship between the FWHM and acceleration voltage. The black point shows the result which set the dipoles to multiple points between scattering positions and the white points shows the result which set the dipole to

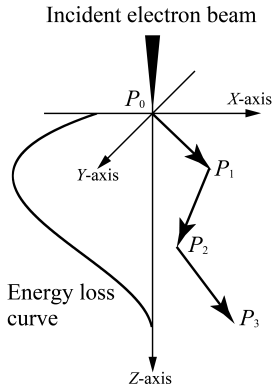

Fig. 1. The schematic of energy loss distribution of electron

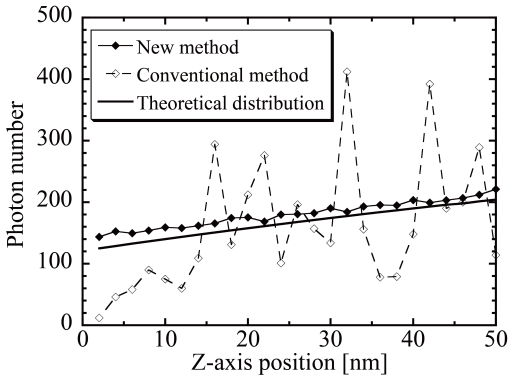

Fig. 2. The relationship between photon number and z-axis position

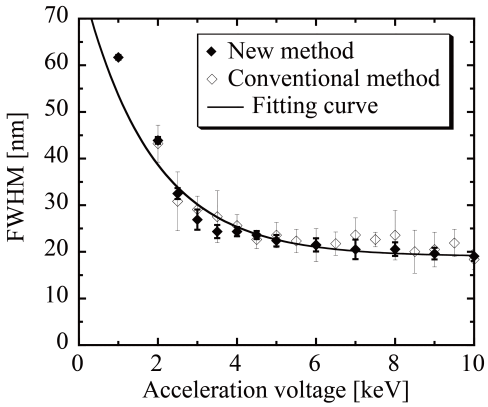

Fig. 3. The relationship between FWHM and acceleration voltage

the middle points between scattering positions. In figure 3, the FWHM become lower with increasing acceleration voltage. There is great variability among the data of conventional method. On the other hand, the data of new method improve this problem. Therefore, the results that set the dipole to multiple points are more accurate than the results that set the dipole to middle point.

5. Conclusion

We analyzed the cathodoluminescence by new analysis method that is combined the Monte Carlo simulation and FDTD method. In this study, we use the energy loss distribution of electrons and we set dipole to the multiple points between the scattering positions. From analysis result, the spot size of cathodoluminescence becomes lower with increasing acceleration voltage.

[1] D. C. Joy, “Monte Carlo modeling for electron microscopy and microanalysis”, OXFORD (1995)

[2] B. G. Yacobi and D. B. Holt “Cathodoluminescence microscopy of inorganic solids” Springer (1990)

3D thickness profile measurement of a thin film

Hang-Eun Joe, Dae Su Kim, and Byung-Kwon Min*

School of Mechanical Engineering, Yonsei University,
50 Yonsei-ro, Seodaemun-gu, Seoul, 120-749, South Korea
TEL: +82-2-2123-6611, FAX: +82-2-365-5595
* e-mail: bkmin@yonsei.ac.kr

Abstract

Thickness of a thin film is an essential design parameter of the metal-film-based devices. Thin film thickness has to be measured accurately that must be controlled to guarantee performance. Although a variety of film thickness measurement methods, such as ellipsometry and transmission electron microscopy, are employed, it is difficult to acquire the 3D thickness profile of a thin film. In this paper, a new method to measure the 3D thickness profile of a thin film is proposed. To effectively measure the difference between two surface profiles, a data alignment method using fiducial marks is proposed. The method is verified experimentally using Cr films.

1. Introduction

Thin-film-based devices are widely used in industrial applications, such as sensors, actuators, transistors, and solar cells. In many cases, the thickness of a thin film is an essential design parameter of the devices that must be controlled to guarantee performance. [1-2]. As electrical devices become more complicated and miniaturized, 3D thickness profile measurement with nanometer accuracy becomes more important.

Optical interferometry can be used to acquire the 3D thickness profile of a film [3]. However, it is difficult to obtain a surface profile of a substrate covered with opaque films using optical interferometry, especially for metal films. The optical methods are affected by optical properties [4]. Therefore, a 3D thickness profile measurement method that can be used regardless of the optical properties of the metal film is required.

In this paper, a new method is proposed to measure the 3D thickness profiles of metal films with nanometer accuracy. The method presented here provides the opportunity to measure the 3D thicknesses of film profiles of thin-film-based devices.

2. Method

A new method is proposed to measure the 3D thickness profiles of metal films using a process of removal of the film. This method consists of surface profile measurement, film removal, and an alignment process. Fig. 1 shows the proposed steps of the process. Fiducial marks are fabricated at the area of interest on the prepared thin film sample (a-b). The top surface profile of the metal film is measured with the marks (b). The surface profile of the substrate over the same area is measured after selective removal of film using wet etching (c). The two profiles are aligned using a linear transformation by matching the three fiducial points. The space between the aligned surface profiles becomes the thickness profile of the film (d).

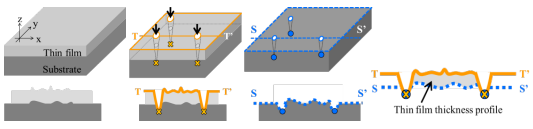

(a) (b) (c) (d)

Fig.1 Diagram of film thickness profile measurement

3. Experiment

Metal films and substrates were prepared to be measured. Silicon wafers were used as substrates and nickel (Ni). The films were deposited by an e-beam evaporator. The fiducial marks were fabricated on the specimen using a focused ion beam system (FIB, SII Nanotechnology SMI 3050). The

surface profiles were measured using atomic force microscopy (AFM, Bruker Dimension 3100). The measured area was 5 μm × 5 μm. The lateral resolution of the AFM was 19.5 nm. Wet etching is an appropriate removal film method since etching selectivity is the property generally valued in thin film technology.

To verify the reliability of the proposed method, the film thickness was also measured by a spectroscopic ellipsometer (SE MG-1000, Nano View). The thickness of the films measured using the proposed method was compared to the thickness measured using the spectroscopic ellipsometer with an identical specimen.

4. Conclusion

The measurement results of the thin metal films are shown in Fig. 2. The calculated average film thickness was 9.0 nm. In order to verify the results, the sample was measured using the spectroscopic ellipsometer. The thickness of the Ni film was measured to be 8.2 nm with the spectroscopic ellipsometer. The average film thickness calculated through the proposed method had an error rate of 8.9 % compared to the spectroscopic ellipsometer result. The results demonstrate that the proposed method is capable of measuring the 3D thickness profile of the thin metal film with nanometer resolution.

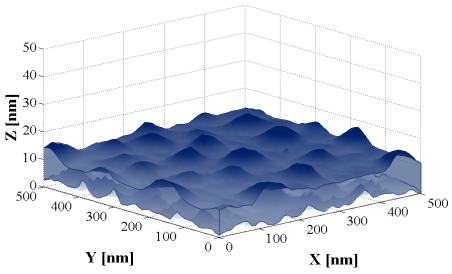

Fig.2 Measurement results of Ni film. The thickness, 8.98nm, had error rate of 8.9 % compared to the spectroscopic ellipsometer result.

References

[1] O'Connor B, Haughn C, An K-H, Pipe K P and Shtein M, Appl. Phys. Lett. 93 (2008) 223304

[2] Zhang X, Choi H, Datta A and Li X, J. Micromech. Microeng 16 (2006) 900-905

[3] Ghim Y-S and Kim S-W, Opt. Exp. 14 (2006) 11885-11891

[4] Nguyen H V, An I and Collins R W, Phys. Rev. B. 47 (1993) 3947-3965

Development of optically controllable electrophoresis with a photoconductive substrate

Taiki Nagashima[A], Wataru Inami[B, C], and Yoshimasa Kawata[A, C]

[A] Faculty of Engineering, Shizuoka University, Japan
[B] Division of Global Research Leaders, Shizuoka University, Japan
[C] Japan Science and Technology Agency, CREST, Japan
e-mail: kawata@eng.shizuoka.ac.jp

Abstract

This paper introduces optically controllable electrophoresis with a photoconductive substrate. This method can manipulate microparticles concurrently without any flow channels. We control moving velocity and direction of microparticles successfully by laser irradiation.

1. Introduction

Micro Total Analysis Systems (μTAS) and Lab-on-a-chip have been developed in a medical and biological applications, and they have been intensively studied. The systems are expected to have more quick procedures and higher functionality.

Objective of this study is to control microparticles in fluid with laser irradiation. By combining property of photoconductive substrate and electrophoresis, we can achieve microparticles operation without flow channel. We believe that this technique contributes to development of the high functionality analysis devices.

2. Principle of optically controllable electrophoresis

Figure 1 shows schematic diagram of optically controllable electrophoresis. We put a few droplet containing microparticles on the photoconductive substrate and generate electrophoresis by applying a voltage to the photoconductive substrate.

Photoconductive substrate is a kind of semiconductor, and its conductance is increased by optical irradiation. When the photoconductive substrate is applied a voltage, potential gradient arises. On the photoconductive substrate, potential gradient is reduced in the laser irradiated area because conductance of irradiated area is increased. $Bi_{12}SiO_{20}$ (BSO) is used as photoconductive substrate[1, 2].

Electrophoresis is the motion of dispersed particles relative to a fluid under the influence of a spatially uniform electric field. The dispersed particles have electric surface charges, on which an external electric field exerts an electrostatic Coulomb force. Velocity and direction of particles depend on potential gradient.

In this study, we change potential gradient on the photoconductive substrate by laser irradiation and control moving direction and velocity of microparticles.

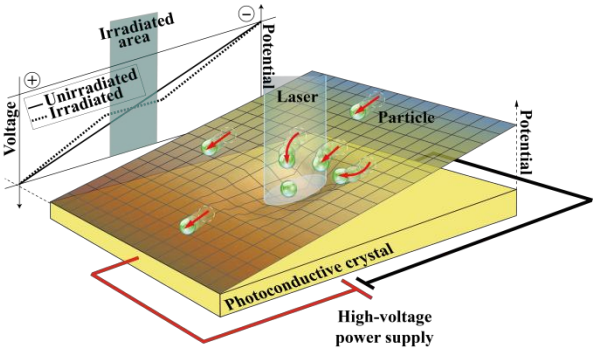

Fig. 1. Schematic diagram of principle of optically controllable electrophoresis. In case of negatively charged microparticles, they move from negative electrode to positive electrode along the potential gradient.

3. Experimental setup

Blue diode laser is used as a light source. Laser power is from 0.1 mW to 0.5 mW, and wavelength is 405 nm. The applied voltage is from 3.0 kV to 5.0 kV. Polystyrene latex particles are used as microparticles, and the sizes are ϕ7 μm and ϕ20 μm. We can control irradiated laser pattern by changing mask pattern and get CCD camera image with scattering light from particles.

4. Results of electrophoresis on the BSO

with laser irradiation

Figure 2 shows CCD images of manipulated microparticles with laser irradiation of different pattern. Microparticles move from negative electrode to positive electrode without laser irradiation.

(a) Line pattern. Particle size: ϕ20 μm.

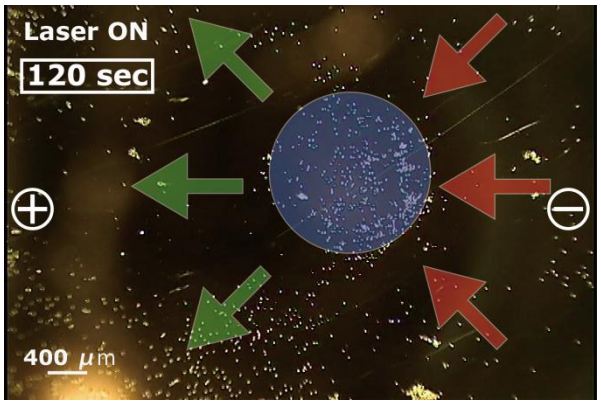

(b) Circular pattern. Particle size: ϕ20 μm.

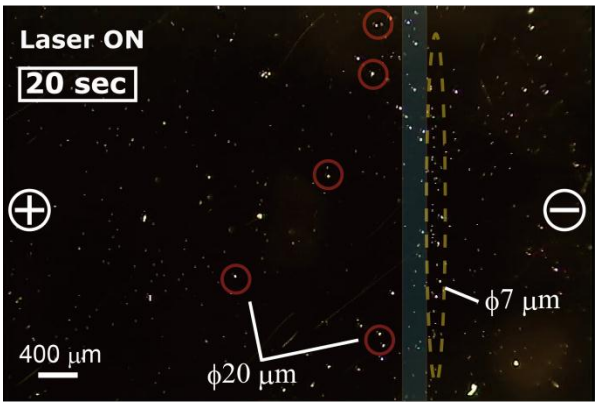

(c) Separate operation. Particle size: ϕ7 and ϕ20 μm.

Fig. 2. CCD images of manipulated microparticles with laser irradiation of different pattern. Particle movements vary with the laser irradiation. Laser power is from 0.1 mW to 0.5 mW, and wavelength is 405 nm. Applied voltage is from 3.0 kV to 5.0 kV.

Figure 2(a) shows particle movements when line pattern laser is irraiated. Because potential gradient in the irradiated area becomes gradual, there is a decrease in the velocity of microparticles and some microparticles stop movements.

Figure 2(b) shows particle movements when circular pattern laser is irraiated. Because potential gradient of the region near the irradiated area becomes steep, microparticles collect around irradiated area.

Figure 2(c) shows microparticle separate operation. Two different sizes of particles are in the fluid (Particle sizes are ϕ7 μm and ϕ20 μm). Verocity of two kinds of particles are different in irradiation area because quantity of electrification charges of particle depend on particle size. Particles of ϕ7 μm stop in front of the irradiation area but particles of ϕ20 μm go through.

5. Conclusion

We controlled moving velocity and direction of microparticles successfully by changing laser irradiation pattern.

We succeeded in separate operation by difference in size of particles.

6. Future work

In this paper, we introduced microparticle operation with unsophisticated laser pattern (line and circular pattern). We will attempt to optically operation with more complicated laser pattern. To accomplish it, preparing higher-accuracy mask pattern and optimization of experimental conditions are necessary.

References

[1] R. E. Aldrich, S. L. Hou, and M. L. Harvill, "Electrical and Optical properties of $Bi_{12}SiO_{20}$ " *J. Appl. Phys.*, **42**, (1971) 493.

[2] M. Peltier and F. Micheron, " Volume hologram recording and charge transfer process in $Bi_{12}SiO_{20}$ and $Bi_{12}GeO_{20}$, "*J. Appl. Phys.*, **48**, (1977) 3683.

Image reconstruction for portable digital holographic microscopy using a glass phase shifter

JaeHyeong Park, Janghyun Cho, Sungbin Jeon, Kyungsoo Lee
Sang-Jo Lee, Byung-Kwon Min*

Department of Mechanical Eng, Nano Manufacturing & Mechatronics, Yonsei University,
308 Industry-University Research Center, 50 Yonsei-ro, Seodaemun-gu, Seoul 120-749, Korea
TEL&FAX : +82-2-2123-6611
*e-mail: bkmin@yonsei.ac.kr

Abstract

Phase shifting in digital holography is used to obtain holographic images clearly and quickly. Because of size and price, conventional phase shifter is not appropriate for portable digital holographic microscope. And then we propose glass phase shifter which is inexpensive and small. We compare Image reconstruction using the conventional with glass. It is shown that glass can be used as phase shifter for portable digital holographic microscope.

1. Introduction

Digital holography is used for a wide range of applications. A lot of techniques deal with holographic microscopy. Digital holographic microscope (DHM) using phase shifter within reference beam path can obtain high-resolution images without noise and calculate numerical reconstruction quickly. In many current DHM, wave plate, phase SLM, and piezo actuator are used as a phase shifter. In particular, because it can be precise control using the same phase shifter the case of phase SLM and piezo actuator has been studied in a lot of digital holographic systems. The case of digital holography using phase shifting the DC component and the imaginary components of the image compared to the general decline, and with the addition of some algorithmic it is possible to remove these almost completely.

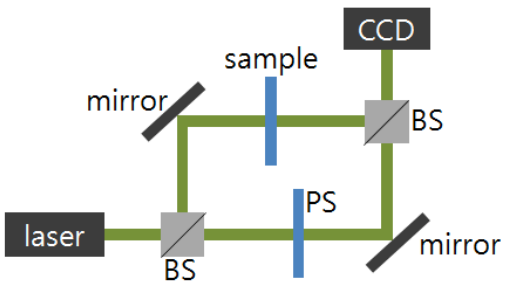

Fig. 1. The schematic view of experimental setup.

But these phase shifters are large and expensive, so in the current phase shifter was developed to use a portable DHM inappropriate. Therefore, the development of a phase shifter for portable DHM is required.

Because glass is inexpensive and easy processing suitable, glass has the advantage of the portable DHM. In this paper, the possibility of flat glass used as a phase shifter is analyzed.

2. Experiment

In this paper, as shown in Fig. 1 By using a beam spliter which separate the reference beam and object beam off-axis digital holographic microscopy methods were used. ND:yag laser (λ=532nm), CCD image sensor (pixel size : 3.45 μm x 3.45 μm) and a test target (USAF 1951 Chart) were used.

First, we put a obstacle on the object beam path, and then obtain the reference image without the use of glass. Second, we put away the obstacle, and then obtain the interference image between the reference beam and object beam. Finally, we put a flat glass which has random thickness on the reference beam path, and then obtain the interference image between the phase shifted reference beam and object beam. Obtained hologram images are numerically reconstructed by using simple direct extraction of unknown phase shift algorithm

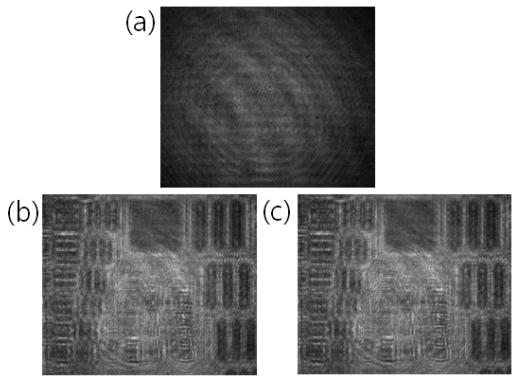

Fig. 2 holograpic images.

with LabVIEW (National Instrument). [1]

3. Results and Discussion

Fig. 2 (a), (b), (c) are respectively reference image, interference image, phase shifted interference image using glass phase shifter. Fig. 3 (a), (b) are reconstructed images using phase SLM and flat glass as phase shifter respectively.

Glass phase shifter and the original were able to confirm that a similar image reconstruction quality. Therefore, we demonstrate that glass phase shifter can be used in a portable DHM.

4. Conclusion

In this research we suggest phase shifter for portable DHM. To use low-priced and lighter phase shifter we certify that glass is good phase shifter for portable DHM.

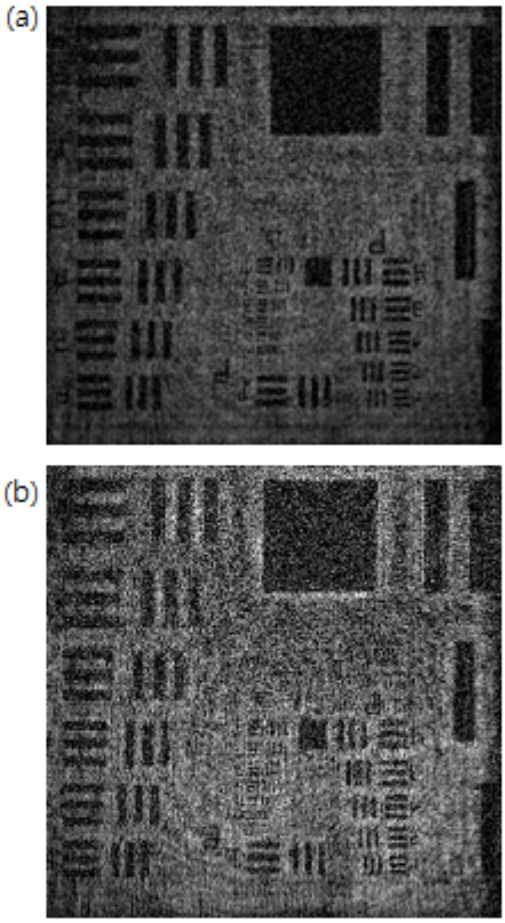

Fig.3 Image reconstruction result using (a) phase SLM, (b) flat glass.

Reference

[1] X. F. Xu, L. Z. Cai, Y. R. Wang, X. F. Meng, W. J. Sun, H. Zhang, X. C. Cheng, G. Y. Dong, and X. X. Shen, Optics Letters **33** (2008) 8

Measurement of electron transmittance of a luminescent thin film with a high electron stopping power layer

Takuya Miyazawa[1], Yotaro Nishimura[1], Wataru Inami[2,3], Yoshimasa Kawata[1,3]
[1]Faculty of Engineering, Shizuoka University, Japan
[2]Division of Global Research Leaders, Shizuoka University, Japan
[3]Japan Science and Technology Agency, CREST, Japan
E-mail: kawata@eng.shizuoka.ac.jp

Abstract

Electron beam may damage specimens at electron beam excitation assisted optical microscope observation. In this paper, we sputtered Au on Si_3N_4 film for stopping electron beam which damage living biological specimens, and measured electron transmittance of this film. Au sputtering is effective to reduce electron transmittance, but there is the difference between measured and calculated data. This major cause is secondary electron emission from Au film.

1. Introduction

We propose electron beam excitation assisted optical (EXA) microscope in which electron beam focused on a luminescent thin film excites nanometric light source near a specimen [1]. This luminescent film is much thin so that electron beam may transmit through this film. Electron beam may damage the specimen. This is a problem to observe dynamic process of living biological specimens. The luminescent film which can stop electron beam is required.

In this study, we cover sputtering film for stopping electron on luminescent film, and then measure of electron transmittance of this film in 1~10 eV.

2. Luminescent film with a high electron stopping layer

We coated Au layer on Si_3N_4 film by radio-frequency sputtering system (CFR-700, SANYU ELECTRON). Au has high electron stopping power and can be sputtered without oxidation. Si_3N_4 film (thickness: 50 nm) is used in EXA microscope as a luminescent film.

3. Setup of electron transmittance measurement

Figure 1 shows schematic diagram of experimental setup of electron transmittance measurement. In this experiment, the scanning electron microscope (SEM, JSM-6390, JEOL) is used. The accelerated electron is focused on luminescent film surface by field lens. Incident electron is measured by the detector fixed on SEM, and transmitted electron is measured by Faraday cup (FC) on specimen mount. The ratio of transmitted electron to incident electron is electron transmittance of the film.

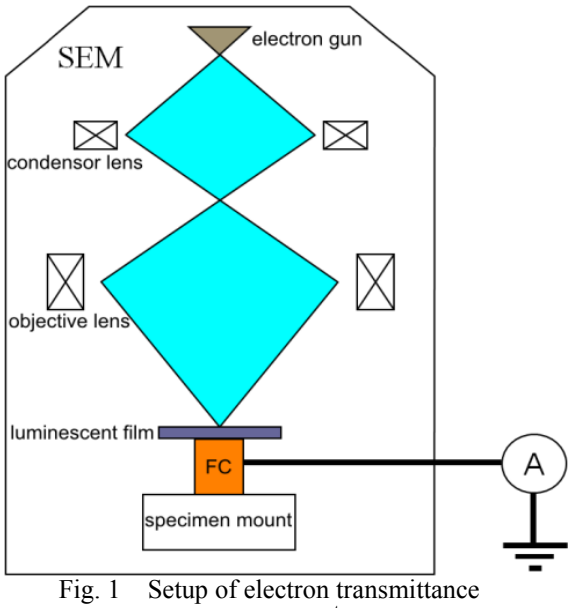

Fig. 1 Setup of electron transmittance measurement

4. Experimental results and discussion

Figure 2 shows electron transmittance as dependent on acceleration voltage; blue line is measured data of Si_3N_4 (which thickness is 50 nm) without Au layer, red line is Si_3N_4 with Au layer which thickness is 20 nm, green line is with Au layer which thickness is 40 nm, and purple line is calculated data with Au layer which thickness is 20 nm by Monte Carlo simulation (MC).

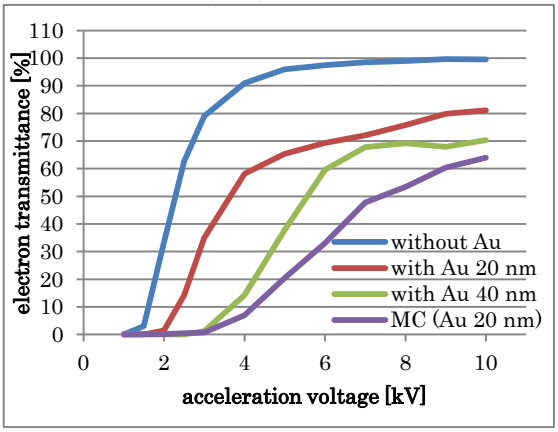

Fig. 2 Electron transmittance of each film

Electron beam is stopped to 1.5 kV without Au, 2.0 kV with Au 20 nm, and 3.0 kV with Au 40 nm. It seems that as Au is thicker luminescent film has a higher electron stopping power. And, electron transmittance is 79 % without Au, 35 % with Au 20 nm, and 1.2 % with Au 40 nm at 3 eV. Electron transmittance is reduced by sputtering Au.

About Si_3N_4 with Au 20 nm, there is difference up to 50 % between measured data and calculated data.

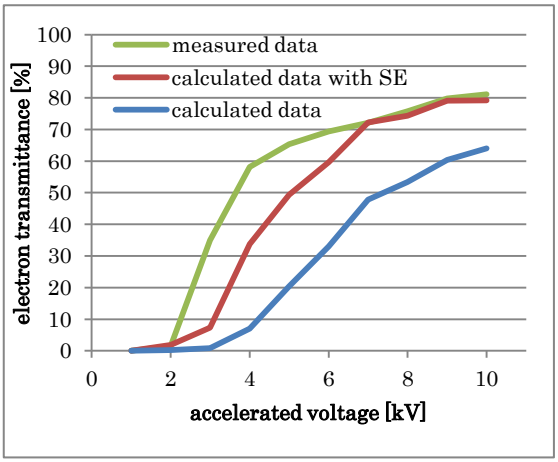

Fig. 3 Comparison of electron transmittance of Si_3N_4 with Au 20 nm

This difference is thought to be due to secondary electron from Au layer. FC used in this experiment can suppress secondary electron outflow from collector, but not inflow from Au layer. Figure 3 shows electron transmittance with Au 20 nm which is measured data, calculated data, and calculated data added secondary electron emission from Au layer.

The approach of secondary electron calculation is roughly. In this study, secondary electron emission is calculated by secondary electron coefficient dependent on primary electron energy and electron energy in position of about 5 nm from the end of Au layer. This length is the secondary electron escape depth of Au.

At high acceleration voltage, calculated data added secondary electron from Au layer fit in measured data. Thus, the major cause of the difference between measured and calculated data is secondary electron from Au film.

5. Conclusion

We sputtered Au on Si_3N_4 film for stopping electron beam which damage living biological specimens, and measured electron transmittance of this film. And, Au sputtering is effective to reduce electron transmittance, but there is the difference between measured and calculated data. This major cause is secondary electron emission from Au film.

Secondary electron energy is up to about 50 eV, but transmitted electron has a few kilo electron volts (keV). So, we have a need to consider the effect on damage to the living cells by the difference of energy electrons have. Additionally, luminescent film with the other materials which have a high electron stopping power is had to be measured.

References

[1] W. Inami, K. Nakajima, A. Miyakawa, and Y. Kawata, “Electron beam excitation assisted optical microscope with ultra-high resolution,” Opt. Exp. **18**, 12897-12902 (2010).